Asian Journal of Chemistry; Vol. 37, No. 8 (2025), 1903-1912

ASIAN JOURNAL OF CHEMISTRY

https://doi.org/10.14233/ajchem.2025.34036

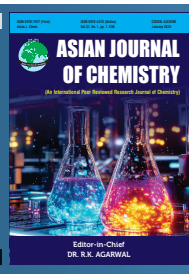

Multifaceted Applications of Chitosan-Coated Zinc Oxide Nanoparticles: Implications for Antibacterial, Antifungal and Anticancer Activity

R. KAVITHA and N. VANITHA*

Department of Microbiology, Hindusthan College of Arts & Science, Coimbatore-641028, India

*Corresponding author: E-mail: vanithanagaraj@hicas.ac.in

Received: 13 May 2025; *Accepted*: 3 July 2025; *Published online*: 31 July 2025; AJC-22069

This study explores the anticancer and antimicrobial effects of zinc oxide nanoparticles (ZnO-NPs) synthesized from chitosan (CS) extracted from crab shells. In this green synthesis approach, chitosan acted as both a reducing and coating agent, resulting in the formation of stable CS-ZnO-NPs. The synthesized CS-ZnO-NPs were characterized by UV-Vis, FTIR, XRD, SEM, TEM and EDX analysis. The UV-Vis analysis indicated a strong absorption peak around 316 nm, confirming the successful synthesis of nanoparticles. The structural analysis conducted through XRD and microscopy showed that the nanoparticles were spherical and hexagonal shapes to cubic, with diameters between 60 and 150 nm. EDX spectra confirmed the elemental composition and fabrication of CS-ZnO-NPs. The biological evaluations showed CS-ZnO-NPs exhibited significant antibacterial and antibiofilm properties against *Escherichia coli*, *Klebsiella pneumoniae* and *Staphylococcus aureus*, along with antifungal effects against *Aspergillus niger*, *Aspergillus flavus* and *Candida albicans*. The anticancer activity of CS-ZnO-NPs was evaluated using the MCF-7 breast cancer cell line. Cytotoxicity assays showed dose- and time-dependent cell death with an IC_{50} of 10 µg/mL. Apoptotic features, such as reduction in cell size and fragmentation of the nucleus, were identified using AO/EB and DAPI staining. Besides that, green synthesized CS-ZnO NPs significantly inhibited migration of MCF-7 cells. The results indicate that chitosan-coated ZnO-NPs demonstrate significant antimicrobial and anticancer properties, positioning them as promising candidates for future biomedical applications.

Keywords: Antimicrobial properties, Antibiofilm effects, Chitosan-coated nanoparticles, *In vitro* studies, MCF-7 cancer cell line.

INTRODUCTION

Chitin is a natural substance made of linked N-acetyl-D-glucosamine units and is known to be the second most common biopolymer after cellulose [1]. The exoskeletons of crustaceans, especially shrimp and crabs, serve as a significant and sustainable resource for the extraction of chitin and its derivatives. Annually, it is anticipated that 6 to 8 million tons of crustacean shell trash are produced [2]. Chitosan, derived from chitin, is often synthesized using chemical or enzymatic deacetylation methods. Chitosan has attracted considerable attention for many biomedical and industrial applications and non-toxic properties [3]. Furthermore, earlier studies have indicated that chitosan exhibits various bioactive properties such as antibacterial [4], antifungal [5], antiviral [6] and larvicidal effects [7].

Natural polymers, such as chitosan, have been increasingly considered safer and more sustainable alternatives in green synthesis processes that aim to address these constraints. Nanoparticles derived from chitosan have potent antibacterial properties, resulting in them being valuable in several biological and industrial applications [8]. In recent years, there has been a growing interest in metal-based nanomaterials due to their distinctive physico-chemical properties and extensive range of applications [9,10]. Numerous fields, such as environmental research, healthcare, agriculture, food safety and the biomedical sectors, might benefit from the use of metal-based nanoparticles. Among the many remarkable qualities of zinc oxide nanoparticles (ZnO NPs) are their low toxicity, eco-friendliness, affordability and biocompatibility. These are some of the most significant aspects of these particles. As a result, ZnO NPs have been thoroughly investigated for their potential applications in biosensing, drug delivery, labeling and therapeutic interventions [10,11]. Gunathilaka *et al.* [12] observed that such materials demonstrate antibacterial, antifungal and mosq-

uitocidal properties, thereby increasing their relevance in the biomedical and public health contexts.

Chitosan-derived nanoparticles have attracted interest for their diverse biological activities, mainly owing to their biodegradability and non-toxic characteristics [13]. The beneficial characteristics of chitosan-based nanomaterials have resulted in their extensive use in food technology, healthcare and agriculture [14]. Chitosan-based nanomaterials are recognized for their antibacterial, antioxidant and immunomodulatory properties [15]. These materials have been thoroughly investigated for their potential in drug delivery applications, particularly in conjunction with metal nanoparticles [16]. Chitosan, a naturally aminated polysaccharide obtained from the exoskeletons of crustaceans and insects, has shown efficacy as a stabilizer and matrix for the synthesis of metal and metal oxide nanoparticles [8].

Chitosan-coated nanoparticles exhibit significant antimicrobial properties, demonstrating efficacy against *Candida* species along with a range of bacterial and fungal pathogens [17]. Recently, it is also demonstrated that chitosan-ZnO nanoparticles can effectively target tumors, exhibit bacteriostatic properties and diminish biofilm formation [3]. Furthermore, recent advancements in hydrothermal synthesis methods have been utilized to form chitosan-encapsulated ZnO nanoparticles that exhibit improved antibacterial effectiveness [8]. This study aims to enhance knowledge of chitosan-coated ZnO nanoparticles through an exploration of their physico-chemical properties, biological performance and environmental compatibility. This study demonstrates their antibacterial, antifungal and apoptosis inducing properties in MCF-7 breast cancer cells, highlighting their multifunctional potential. It contributes significantly to the current development of sustainable nanomaterials for therapeutic and medicinal applications.

EXPERIMENTAL

Crab shell collection and preparation: Mud crab (*Scylla serrata*) shells were procured from a local market in Coimbatore, India. To preserve freshness during transportation, the samples were stored on ice until arrival at the laboratory. Upon receipt, the crab exoskeletons were carefully chopped into smaller fragments using a meat tenderizer. A 20 g quantity of crushed shell material was carefully weighed, labeled and oven-dried at 65 ºC for 4 days to achieve a consistent weight. The moisture content was calculated by subtracting the original wet weight from the final dry weight. The average moisture level of the crab shell samples was deter-mined to be 15.66%.

Chitosan extraction and purification from crab shell: The recovery of chitosan from crab shells began with thoroughly washing the crushed exoskeletons using distilled water. The cleaned material was then transferred into 1000 mL beakers containing boiling NaOH solutions at concentrations of 2% and 4% (w/v) and heated for 1 h to remove proteins and sugars, effectively isolating crude chitin. The 4% NaOH concentration aligns with the method used by the Sonat Corporation [18]. After boiling, the beakers were removed from the hot plate and allowed to cool at room temperature for 30 min, following the approach described by Lamarque *et al*. [19]. The softened exoskeletons were further crushed into smaller fragments (0.5-5.0 mm) using a meat tenderizer. The demineralization of crude chitin was carried out using 1% HCl (v/v) and 2% NaOH, as per the method reported by Huang *et al*. [20]. Subsequently, the demineralized chitin was subjected to deacetylation by adding 50% NaOH and boiling the mixture at 100 ºC for 2 h. The reaction mixture was then cooled for 30 min at room temperature. This deacetylation process was repeated to ensure the conversion of chitin into chitosan, yielding a creamy-white final product.

Preparation of chitosan-coated zinc oxide nanoparticles (CS-ZnO-NPs): To prepare a 1.0% (w/v) chitosan solution, chitosan was dissolved in 1% (v/v) acetic acid while stirring constantly until fully dissolved. Following this, 45 mL of 0.1 M $Zn(CH_3COO)_2{\cdot}2H_2O$ was slowly added to 5 mL of chitosan solution. The pH of the resulting mixture was adjusted to 9- 10 using 0.1 M NaOH, with continuous stirring maintained for 4 h at 85 ºC. After the reaction, the mixture underwent drying at 120 ºC for 2.5 h. This was followed by annealing at 450 ºC for 4 h to yield chitosan-coated zinc oxide nanoparticles (CS-ZnO-NPs) [21-23].

Characterization: The physico-chemical characteristics of the chitosan-zinc oxide nanoparticles (CS-ZnO-NPs) were initially confirmed by UV-visible spectrophotometry. Further morphological and structural analyses were conducted using scanning electron microscopy (SEM), transmission electron microscopy (TEM) and energy-dispersive X-ray analysis (EDAX). X-ray diffraction (XRD) was employed to evaluate the crystalline structure and phase purity of the synthesized nanoparticles. The particle size and the presence of functional chemical groups were characterized using Fourier-transform infrared (FTIR) spectroscopy, following the protocol outlined by Ramimoghadam *et al*. [24].

Evaluation of the antibacterial effect of CS-ZnO-NPs on bacterial pathogens: The antibacterial activity of chitosan-zinc oxide nanoparticles (CS-ZnO-NPs) was assessed using the agar well diffusion method on sterile Müller-Hinton agar plates. A 0.1% inoculum suspension of *E. coli*, *K. pneumoniae* and *S. aureus* was used for inoculation. Wells were aseptically punched into the agar and CS-ZnO-NPs were introduced at the concentrations of 10, 15 and 30 μg mL^{-1}. Following incubation, the diameter of the inhibition zones surrounding each well was measured to evaluate antibacterial efficacy, as described by Gulati *et al*. [25].

Antibiofilm activity: The antibiofilm activity of CS-ZnO-NPs was evaluated by cultivating *E.coli*, *K. pneumoniae* and *S. aureus* individually in glass test tubes containing nutrient broth. An equal volume (10 mL) of overnight bacterial culture and sterile nutrient broth was mixed and treated with CS-ZnO-NPs at a concentration of 30 μg mL^{-1}. The cultures were incubated for 48 h. After incubation, the contents were centrifuged at 5000 rpm for 5 min and the supernatant was discarded. The biofilm-forming cells adhered to the glass surface and were washed three times with sterile distilled water. Subsequently, each tube was stained with 1 mL of 0.1% crystal violet solution and incubated at room temperature for 30 min. Excess stain was removed and the tubes were washed thrice with distilled

water and gently dried. Photographs were taken to document the extent of biofilm formation on the inner surface of the tubes.

Antifungal activity: The antifungal activity of the CS-ZnO-NPs was assessed using the agar well diffusion method, as described by Gizaw *et al*. [26]. Subcultured *A. niger*, *A. flavus* and *C. albicans* were incubated on Potato Dextrose Agar (PDA) plates at 35 ºC for three days. To prepare the fungal inoculum, 10 mL of potato dextrose broth was inoculated with three-day old cultures of each fungal strain. The surface of PDA plates was uniformly swabbed with the prepared inocula. Using sterile pipette tips, four wells (6 mm diameter) were made in each plate. CS-ZnO-NPs (10, 15 and 30 mg/mL) were loaded into the wells (0.1 mL/well), alongside DMSO as a negative control and fluconazole (1 mg/mL) as a positive control. After allowing the plates kept at room temperature for 1 h to permit diffusion, they were incubated at 28-30 ºC for 92 h. Antifungal activity was evaluated by measuring the diameter of the inhibition zones in millimeters. The percentage of inhibition was calculated using a standard formula, following the method of Urnukhsaikhan *et al*. [27].

$$\text{Inhibition (\%)} = \frac{\text{ZOI of samples (mm)}}{\text{ZOI of standard drug (mm)}} \times 100$$

Anticancer activity of CS-ZnO NPs against human breast cancer cells

Cell culture: The MCF-7 breast cancer cell line was sourced from the National Centre for Cell Sciences (NCCS) in Pune, India. These cells were cultured in Dulbecco's Modified Eagle Medium (DMEM) with 10% fetal bovine serum (FBS) and maintained at 37 ºC in a CO_2-incubated, humidified environment.

MTT assay: The cytotoxicity of CS-ZnO-NPs was assessed using the MTT assay. A549 cells were seeded in 96-well plates to form confluent monolayers. Different concentrations of CS-ZnO-NPs (0-100 µg/mL) were added to the cells and cell viability was determined by evaluating the reduction of the tetrazolium salt MTT [3-(4,5-dimethylthiazol-2-yl)-2,5-diphenyl tetrazolium bromide], purchased from Sigma Chemical Co., St. Louis, Missouri, USA. This reduction occurs through the action of succinate dehydrogenase, an enzyme found in the mitochondria, resulting in the formation of formazan crystals that indicate viable cells. Each concentration was tested in triplicate to ensure consistency and reliability of the results. The 50% inhibitory concentration (IC_{50}), which represents the concentration required to decrease cell viability by 50%, was determined using regression analysis. The percentage viability was calculated from the optical density (OD) values using the following formula:

$$\text{Viability (\%)} = \frac{\text{OD value of experimental sample}}{\text{OD value of experimental control}} \times 100$$

Morphological analysis: Human cancer cells, seeded onto coverslips at a density of 1×10^5 cells per coverslip, were exposed to CS-ZnO-NPs at concentrations of 10, 25 and 50 µg/mL for 24 h. After treatment, the cells were fixed using a 3:1 (v/v) ethanol and acetic acid solution. The treated coverslips were then carefully transferred to glass slides for subsequent morphometric analysis. To evaluate the cell morphology, three monolayers from each experimental group were captured using bright-field inverted light microscopy at a 40x magnification on a Nikon (Japan) microscope. This technique allowed for the detailed observation of any morphological changes in the cells following treatment.

Analysis of apoptotic cell death using fluorescence microscopy: For staining, a mixture of 1 µL distilled water, 100 mg/mL acridine orange (AO) and ethidium bromide (EtBr) was prepared. A 0.9 mL solution containing 1×10^5 cells was added to the mixture on clean coverslips. Prior to staining, cancer cells were treated with different concentrations of CS-ZnO-NPs, then collected and washed with phosphate-buffered saline (PBS, pH 7.2). The cells were treated with 10 µL of AO/EtBr solution for 2 min, washed twice with PBS and observed under a Nikon Eclipse fluorescence microscope at 40x magnification using a 480 nm excitation filter. In a separate procedure, cells were grown on glass coverslips in six-well plates and exposed to varying concentrations of CS-ZnO-NPs for 24 h. After treatment, the cells were fixed with a 3:1 (v/v) methanol-acetic acid solution, washed with PBS and stained with DAPI (1 mg/mL) for 20 min in dark. Images were captured using a fluorescent microscope with the appropriate excitation filter.

Statistical analysis: All *in vitro* experiments were carried out in triplicate, with each experiment repeated a minimum of three times. Data were analyzed using SPSS version 17.0 and a p value of < 0.01 was regarded as statistically significant.

RESULTS AND DISCUSSION

UV-visible spectroscopy: The UV-vis spectrophotometric analysis of CS-ZnO-NPs revealed a peak at approximately 316 nm, with the symmetrical band structure suggesting uniform dispersion and affirming particle stability (Fig. 1). Prior studies have recognized a specific absorption band for ZnO NPs within the 280-400 nm range [28]. ZnO/CS composites have demonstrated notable absorption in the range of 350 to 380 nm [29], whereas ZnO-NPs and CS-ZnO-NPs displayed peaks at 375 and 357 nm, respectively [30]. The spectra indicate the successful integration of ZnO nanoparticles onto the chitosan surface, resulting in the formation of ZnO-CS composite. The detected blue shift in the UV spectra indicates the formation of the CS-ZnO nanocomposite, probably attributed to the presence of ZnO [31,32]. Oh *et al*. [33] also observed a significant peak at 320 nm in the UV-visible spectrum of chitosan nanoparticles.

FTIR studies: The FTIR transmittance spectra of CS-ZnO-NPs, illustrated in Fig. 2, display distinct bands ranging from 4000 to 600 cm^{-1}, with significant peaks at 3322.75, 2917.77, 2135.78, 1644.02, 1390.42, 1149.37, 1034.42, 893.84, 813.81 and 753.06 cm^{-1}. The broad band at 3322.75 cm^{-1} and the minor peak at 1390.42 cm^{-1} are associated with O–H stretching, which is the characteristic of alcohol and phenolic compounds. The peaks observed at 2917.77 and 753.066 cm^{-1} are indicative of C-H stretching in alkanes. The peak observed at 2135.78 cm^{-1} is associated with C-H modes in aromatic compounds. The peaks observed at 1644.02, 893.844 and 813.813 cm^{-1} correspond to C=C stretching in alkenes.

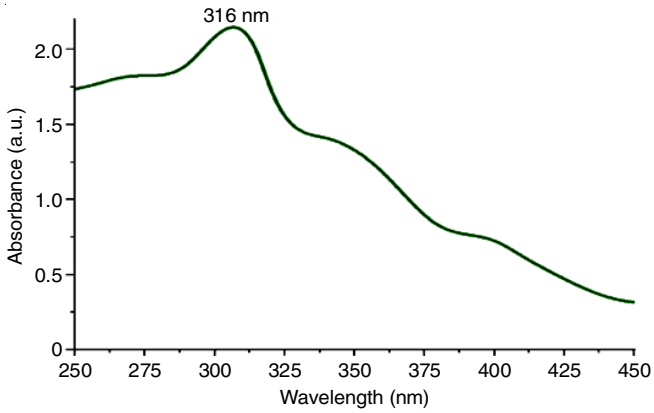

Fig. 1. UV-visible spectrum of CS-ZnO NPs

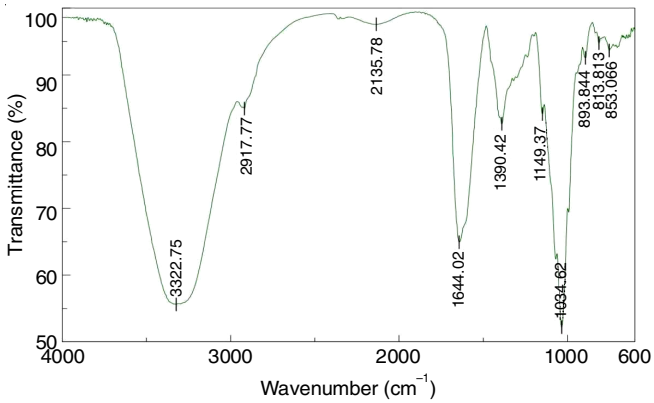

Fig. 2. FT-IR spectrum of CS-ZnO NPs

The stretching vibrations of C-O in primary and secondary alcohols are observed at 1149.37 and 1034.42 cm^{-1}, respectively. Previously, observed pronounced bands in the 1250-1100 cm^{-1} range, linked to C–O stretching, indicating the organic characteristics of CS-ZnO-NPs and their eco-friendly synthesis [34].

X-ray diffraction studies: The phase and crystal structure of CS-ZnO-NPs were examined using X-ray diffraction, which showed a clear and specific pattern (Fig. 3). The CS-ZnO-NPs displayed peaks at 2θ values of 31.97º, 34.81º, 36.87º, 47.98º,

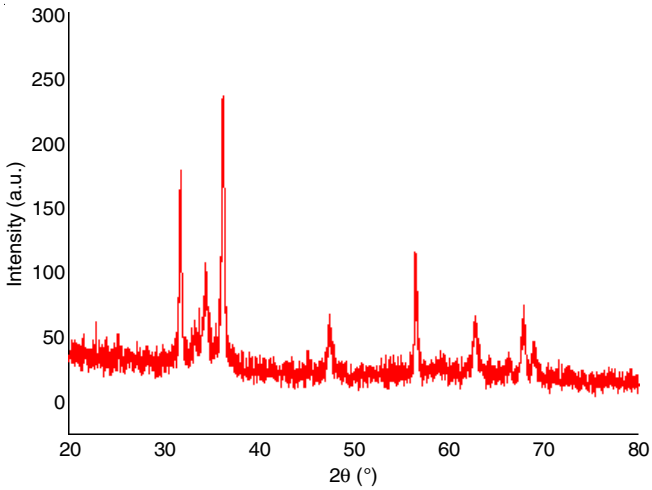

Fig. 3. XRD spectrum of CS-ZnO NPs

56.91º, 62.91º, 66.93º, 68.51º, 69.62º, 72.74º and 77.87º, which correspond to the (*hkl*) planes (100), (002), (101), (102), (110), (103), (200), (112), (201), (004) and (202). The peaks corresponded with JCPDS card No. 36-1451, thereby confirming the existence of a hexagonal phase structure in the synthesized ZnO nanoparticles [35].

A broad diffraction peak in the chitosan-ZnO nanocomposite pattern suggested the semi-crystalline nature of chitosan and validated the successful incorporation of hexagonal ZnO nanoparticles into the chitosan matrix [36]. The XRD patterns clearly illustrated the successful synthesis of CS-ZnO NPs. The Scherrer's formula was employed to calculate the crystallite size [37]. The diffraction peaks associated with cotton fabric and the CS-ZnO nanocomposite indicated that the CS-ZnO coating was effectively applied to the cotton fabric [30].

Morphological studies: The morphological characteristics of CS-ZnO-NPs were examined through scanning electron microscopy (SEM) to determine their shape. The SEM images demonstrated that the synthesized nanoparticles displayed both spherical and hexagonal morphologies, with some agglomeration noted, as shown in Fig. 4. The particles exhibited a uniform

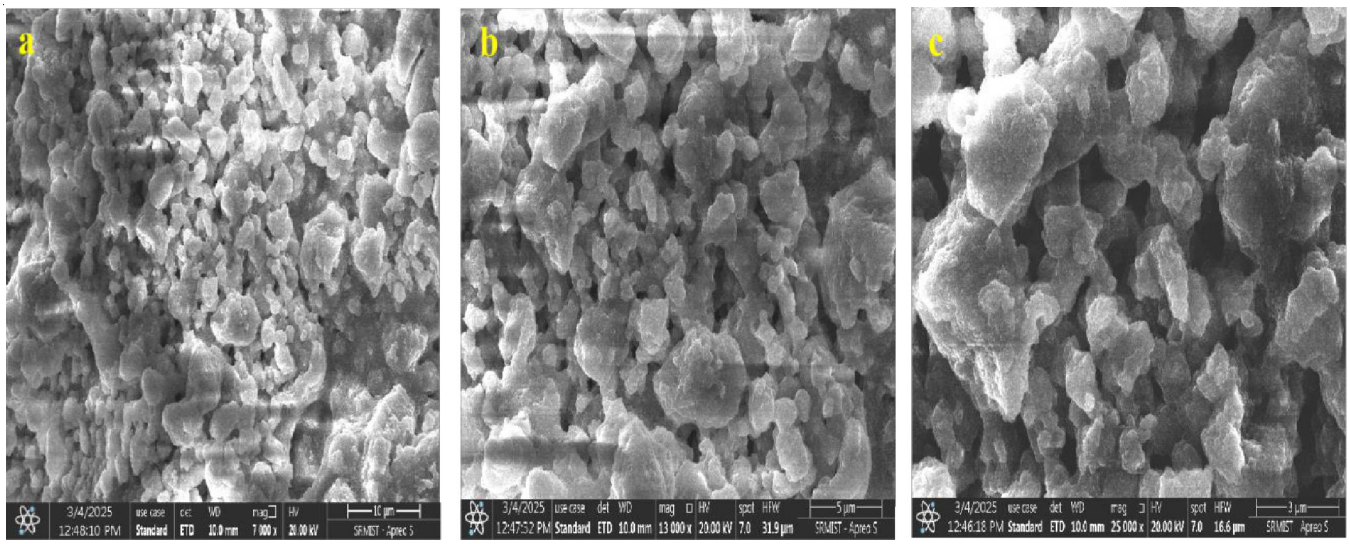

Fig. 4. Scanning electron microscopy of CS-ZnO-NPs (a) 7000× (b) 13,000× and (c) 25,000× magnifcation

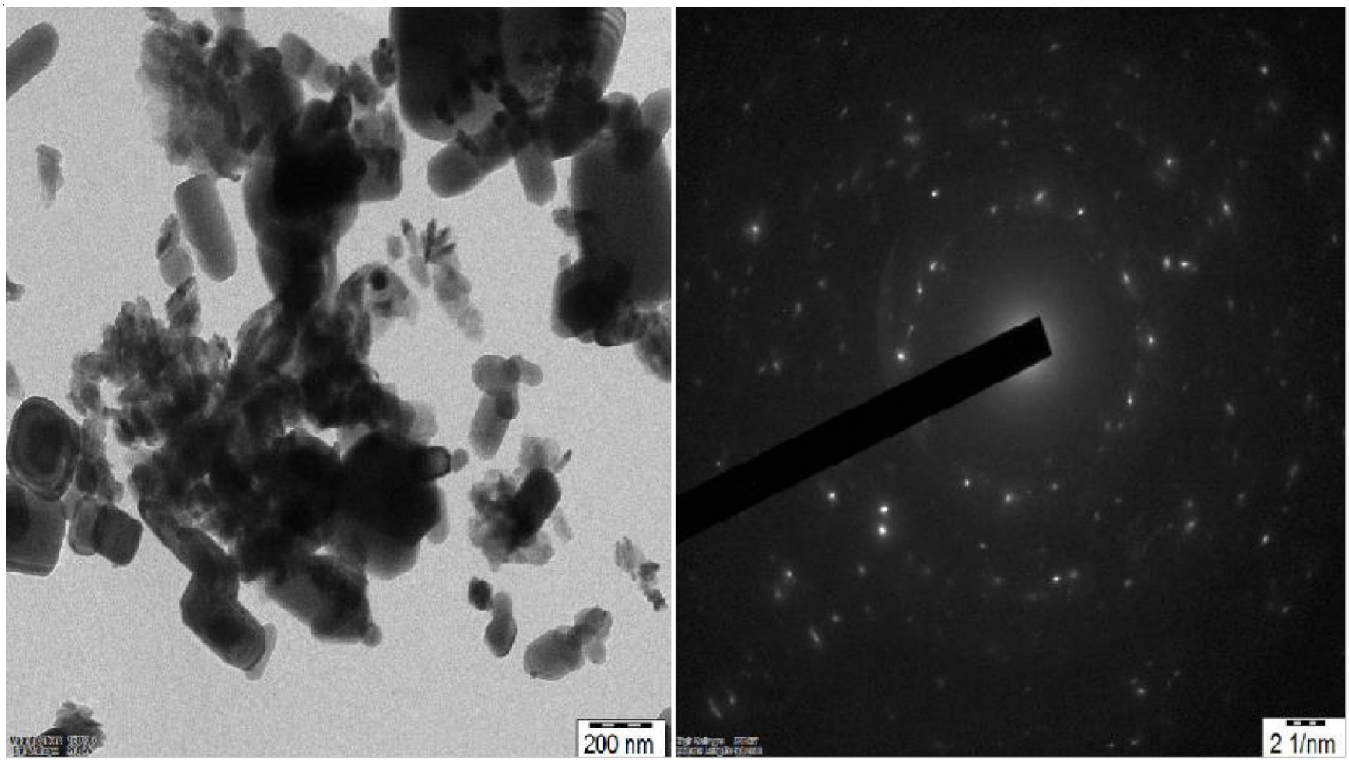

Fig. 5. Transmission electron microscopy of CS-ZnO-NPs

distribution, with sizes varying from 60 to 150 nm and agglomerates can be observed in Fig. 4a-c. The results align with earlier works also [38-40]. The SEM analysis validated the spherical morphology of the ZnO nanoparticles, distinguished by smooth edges, consistent with previous reports [41,42].

The surface structure and particle size of CS-ZnO-NPs were examined through transmission electron microscopy (TEM), as illustrated in Fig. 5. The TEM image shows the agglomerated particles that display both spherical and hexagonal shapes, with an average particle size of 60-150 nm. High-resolution transmission electron microscopy (HR-TEM) was utilized to verify the spherical morphology of the nanoparticles. The synthesis of chitosan-coated ZnO nanoparticles (CS-ZnO-NPs) was validated by comparing particle sizes obtained through TEM and X-ray diffraction, confirming the successful fabrication of the nanoparticles. The results align with the earlier research, notably the study conducted by Pillai *et al.* [43].

EDX spectrum of CS-ZnO-NPs: The elemental composition of CS-ZnO-NPs was examined through energy dispersive X-ray spectroscopy (EDS), which indicated the presence of Zn, O and Ca atoms. Fig. 6 illustrates the stoichiometric mass percentages of Zn (68%), O (20%) and Ca (12%). The EDS results of this study aligned with the earlier findings [44,45]. The findings indicated that these nanoparticles exhibit encouraging characteristics for possible biomedical uses, especially in drug delivery systems. After characterization, the chitosan nanoparticles were subjected to *in vitro* biological assays to assess their anticancer, antibacterial and antifungal activities.

Antibacterial activity: The antibacterial activity of CS-ZnO-NPs was assessed at concentrations of 10, 15 and 30 µg/mL against bacterial pathogens such as *E. coli*, *K. pneumoniae*

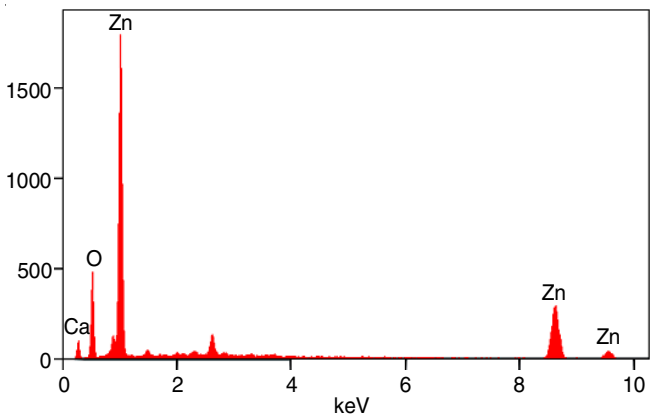

Fig. 6. Energy dispersive X-ray analysis of CS-ZnO NPs

and the *S. aureus* complex. Following a 24 h incubation period, the inhibition zones were measured, resulting in the following values: *E. coli* (6.7, 12.5, 22 mm), *K. pneumoniae* (7, 13, 21.9 mm) and *S. aureus* (7.1, 15.1, 24.5 mm). The data show that the inhibition of bacterial growth increased with higher concentrations of CS-ZnO-NPs. The CS-ZnO nanocomposites exhibited significant antibacterial activity, especially against *S. aureus*, a Gram-positive bacterium [46]. ZnO-NPs demonstrated a bacteriostatic effect on *E. coli* and *P. aeruginosa* while exhibiting bactericidal effects on *S. aureus* and *K. pneumoniae* [47]. Furthermore, the photocatalytic and antibacterial properties of chitosan nanomaterials concerning methylene blue have also been documented [48]. The CS- ZnO nanocomposites exhibited the most significant inhibition zone against *E. coli*, with an inhibition zone of 25.5 mm, followed by *K. pneumoniae* (24.5 mm), *S. aureus* (22.5 mm) and *B. subtilis* (21 mm) [49].

Antibiofilm activity of CS-ZnO-NPs: The anti-biofilm activity of biosynthesized CS-ZnO-NPs was assessed against *E. coli*, *K. pneumoniae* and *S. aureus* strains through the crystal violet assay. Biofilm was allowed to form in glass test tubes before treating with CS-ZnO-NPs at a concentration of 30 µg/mL. The bacterial strains formed biofilms on the glass surfaces, as indicated in Fig. 7a-c. Following treatment with the nanoparticles, a notable decrease (75-90%) in biofilm formation was observed, demonstrating that the biosynthesized nanoparticles successfully interfered with the biofilms. Without treatment, the bacteria formed a clear ring at the top of the liquid in the glass test tubes, but this ring was much smaller after being treated with CS-ZnO-NPs. This finding demonstrates the capability of chitosan nanoparticles to inhibit bacterial growth and biofilm formation, especially in *S. aureus* strains [50]. Hsueh *et al*. [51] reported a reduction in biofilm formation in *B. subtilis* when treated with low concentrations of ZnO NPs, resulting in smoother surface structures. Furthermore, ZnO NPs at a concentration of 50 µg/mL were the most effective in inhibiting biofilm formation in *E. coli* when compared to *B. subtilis*, thereby strengthening the potent biofilm-disrupting capabilities of ZnO-based nanocomposites [52].

Antifungal activity: The CS-ZnO-NPs demonstrated significant antifungal activity against *A. niger*, *A. flavus* and *C. albicans* by compromising the integrity of the fungal cell membrane. *In vitro* testing revealed inhibition zones for *A. niger* at concentrations of 10 mg/mL, 15 mg/mL and 30 mg/mL, measuring 5.2, 7.2 and 9.5 mm, respectively. For *A. flavus*, the inhibition zones were 6.1, 8.8 and 10.6 mm and for *C. albicans*, they were 6.6, 8.7 and 10.4 mm at the same concentrations. These findings suggest that CS-ZnO-NPs exhibit broad-spectrum antifungal activity and could serve as promising candidates for novel antifungal agents. Previous studies have also highlighted the antifungal potential of ZnO nanoparticles, showing effective activity against *C. albicans* at a concentration of 200 µg/mL [53]. In comparison, ZnO-chitosan nanocomposites demonstrated a lower minimum inhibitory concentration (MIC) of 75 µg/mL, indicating enhanced antifungal properties [54]. Moreover, chitosan-ZnO composites have been found to show greater antifungal effects against *A. flavus* and *A. parasiticus* [55].

Exploring the anticancer potential of CS-ZnO-NPs against MCF-7 cells

MTT assay: The potential cytotoxicity of CS-ZnO-NPs (up to 100 µg/mL) was evaluated using the MTT assay over 24 h. The results indicated that CS-ZnO-NPs significantly inhibited cell proliferation, with the degree of inhibition increasing with higher concentrations. The IC_{50} values, presented in Table-1, revealed that CS-ZnO-NPs had an IC_{50} of 10 µg/mL for breast cancer cells, while the standard treatment, doxorubicin, showed an IC_{50} of 4.5 µg/mL. This suggests that CS-ZnO-NPs exhibit notable efficacy against breast cancer cells, potentially outperforming traditional therapies. Similar studies have reported comparable outcomes. For instance, berberine-decorated zinc oxide-loaded chitosan nanoparticles showed an IC_{50} of 7.41 µg/mL against MCF-7 cells [56]. Chitosan-ZnO NPs also demonstrated cytotoxicity in A549 cells, with an IC_{50} of 20 µg/mL [3]. These findings are consistent with previous research on the anticancer effects of nanoparticles [57]. Furthermore, other studies have highlighted the anticancer potential of chitosan-

TABLE-1
CYTOTOXIC ACTIVITY OF CS-ZnO-NPs (µg/mL)

Sample	MCF 7 (breast cancer cells) IC_{50}
CS-ZnO NPs	10 ± 1.2 µg/mL
Doxorubicin (std.)	4.5 ± 0.3 µg/mL

IC_{50} = values of respective sample at 24 h

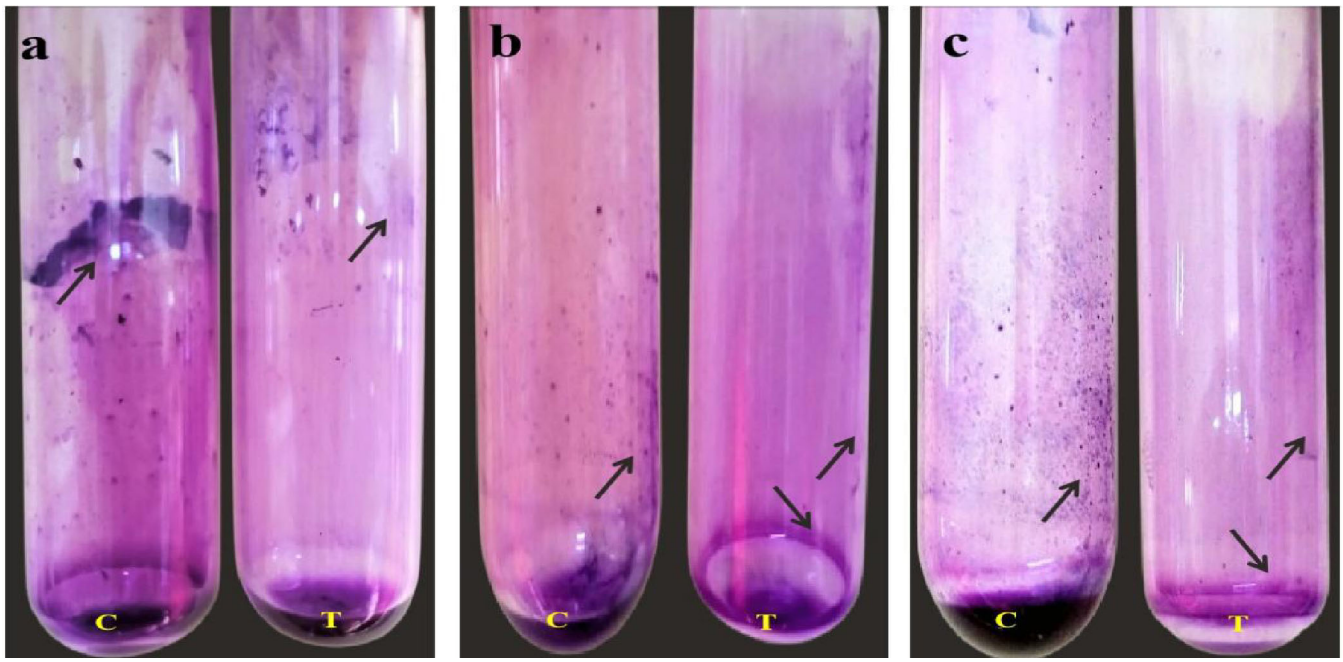

Fig. 7. Antibiofilm activity of CS-ZnO-NPs (30 µg/mL concentration) against (a) *E. coli*, (b) *K. pneumoniae* and (c) *S. aureus*

based nanocomposites, such as chitosan/PVA/copper oxide, against MCF-7 cell viability [58].

Morphological analysis: MCF-7 cancer cells were treated with the IC_{50} concentration of CS-ZnO-NPs for 24 h, resulting in significant morphological changes, as depicted in Fig. 8. The appearance of the treated cells altered with increasing concentrations of CS-ZnO-NPs, showing more pronounced cytotoxicity at higher doses. Significant effects included shrinkage of cells, formation of membrane blebs, cytoskeletal rearrangement and a significant reduction in viable cell numbers. These findings strongly indicate that CS-ZnO-NPs caused cell death in MCF-7 cells, as shown in Fig. 8b-d. In contrast, the untreated control cells showed no visible morphological differences (Fig. 8a). Similarly, previous studies have reported significant cytotoxic effects of chitosan-based nanoparticles, such as Ch-ZnO-NPs and chitosan silver nanoparticles, on the MCF-7 breast cancer cells [59,60]. Moreover, the present results demonstrated a cytotoxic effect of CS-ZnO-NPs up to 85%, surpassing the previous findings [61,62].

Fluorescence microscopic analysis of AO/EtBr and DAPI staining for nuclear fragmentation: Fluorescence microscopy was employed to assess the apoptotic impact of CS-ZnO-NPs on selected cancer cell lines. Green fluorescence indicated living cells, while dead cells were showed by characteristic acridine orange staining. Fig. 9a shows an unusual abundance of viable cells in the untreated control cells. On the other hand, the MCF-7 cells treated with CS-ZnO-NPs indicated an increased presence of cells undergoing apoptosis and the formation of apoptotic bodies. These were distinguishable by their unique characteristics, including nuclear condensation, structural damage to the nucleus and the formation of blebs, which appeared as bodies emitting an orange/red colouration (Fig. 9b-d). It appears that the treatment caused apoptotic changes in MCF-7 cells, resulting in noticeable alterations that suggest apoptosis when examined.

Furthermore, DAPI staining was used to assess the effectiveness of CS-ZnO-NPs. Fig. 10 illustrates that MCF-7 cells treated with CS-ZnO-NPs displayed bright spots, indicating clumped chromatins and damaged nuclear morphology (Fig. 10b-d). In contrast, untreated cells (Fig. 10a) did not show significant changes. The fluorescence microscopy findings highlight the potential of CS-ZnO-NPs as a promising therapeutic agent for cancer treatment, demonstrating substantial growth inhibition in MCF-7 cancer cells. These findings align with previous studies that report the apoptosis-mediated cytotoxicity of ZnO NPs in various cancer cell lines, including breast cancer [63,64]. Moreover, the results suggest that phyto-fabricated ZnO nanoparticles may enhance breast cancer therapies by targeting the anti-apoptotic mechanisms in cancer cells [65].

Conclusion

This study successfully demonstrated the biosynthesis of zinc oxide nanoparticles (ZnO NPs) using chitosan (CS) extracted from crab shells as a capping agent. The resulting CS-ZnO-NPs were small size, stable and structural and elemental characteristics were confirmed using multiple characterization techniques including UV-vis spectroscopy, FTIR, XRD, SEM, TEM and EDX analysis, indicationg the successful of the bio-

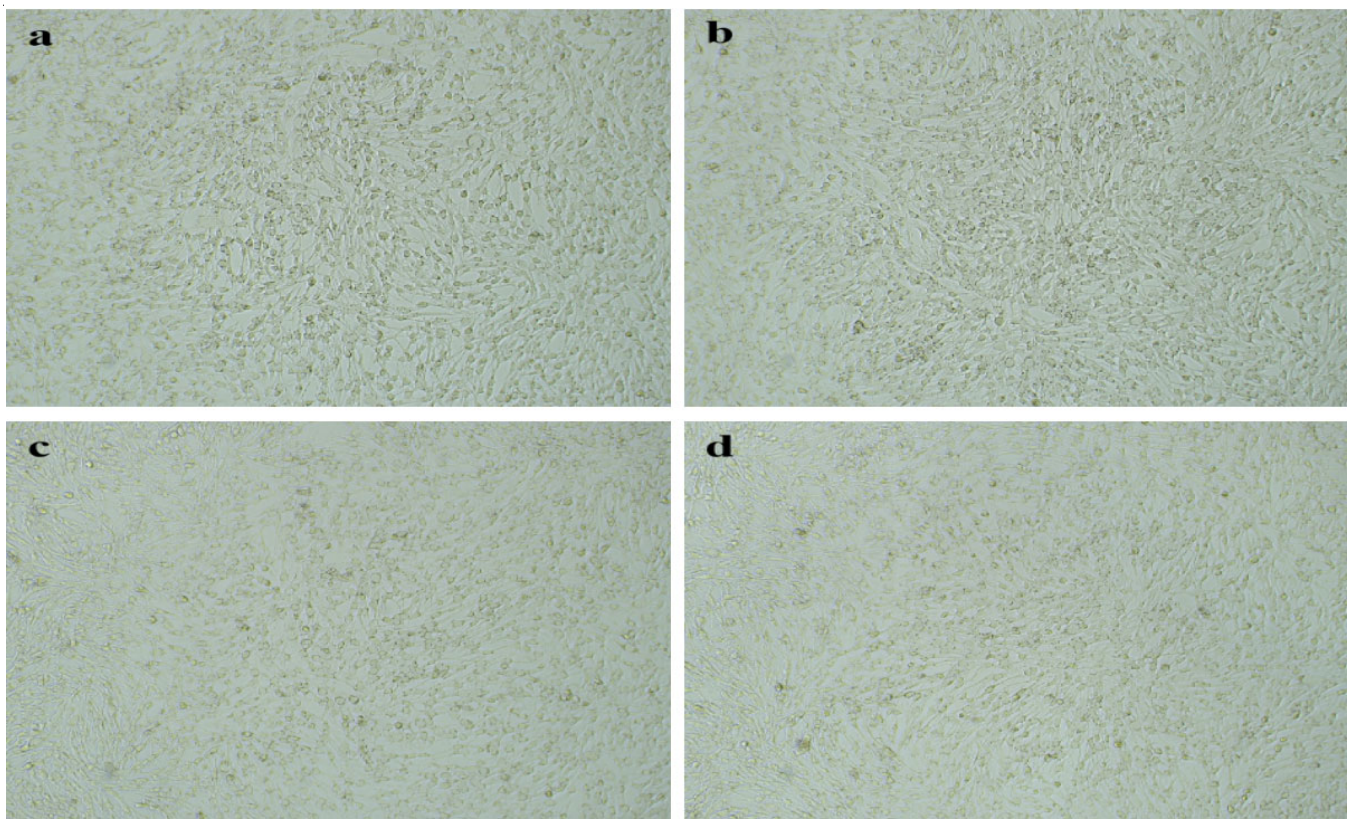

Fig. 8. Morphological analysis of CS-ZnO-NPs treated MCF 7 cells for 24 h (a) Control (b)10 µg/mL (c) 25 µg/mL (d) 50 µg/mL

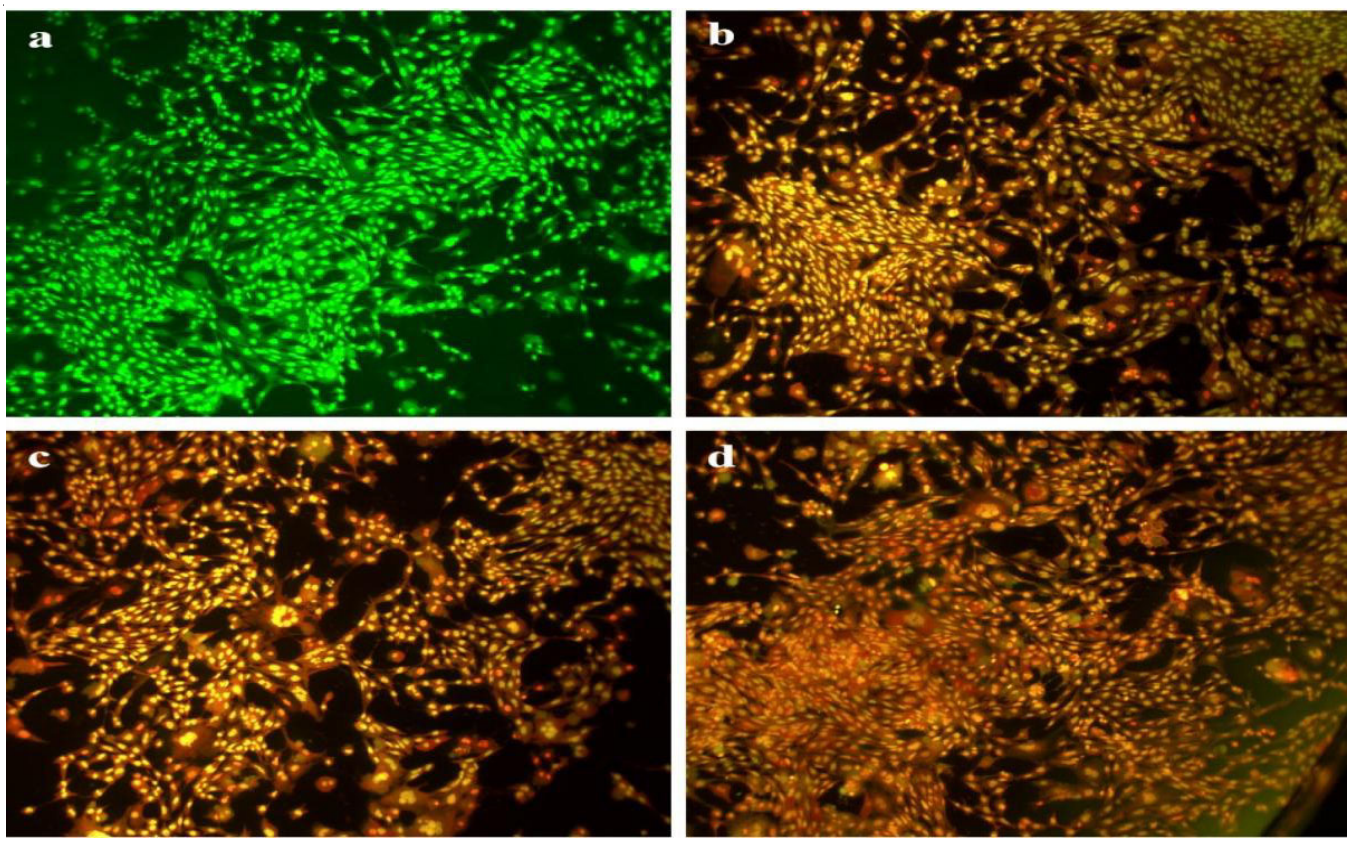

Fig. 9. Assessment of apoptosis in MCF-7 cells using AO/EtBr staining after treatment with CS-ZnO-NPs (a) Control (b) 10 µg/mL (c) 25 µg/mL (d) 50 µg/mL

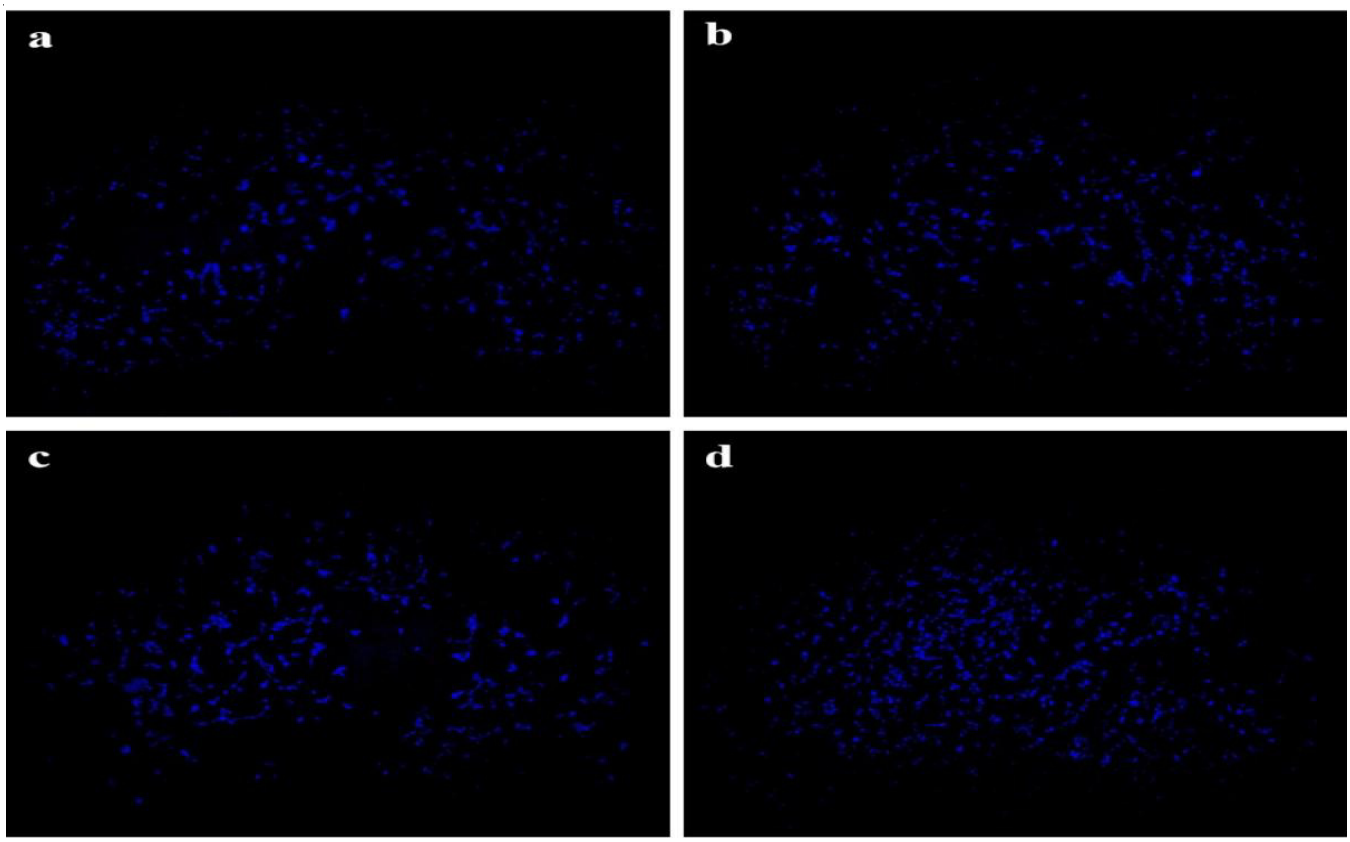

Fig. 10. Assessment of apoptosis in MCF-7 cells using DAPI staining after treatment with CS-ZnO-NPs (a) Control (b) 10 µg/mL (c) 25 µg/mL (d) 50 µg/mL

synthesis process. The results revealed that the CS-ZnO-NPs exhibited outstanding antibacterial and antifungal properties. Moreover, these nanoparticles significantly inhibited the proliferative and migratory activities of human breast cancer MCF-7 cells, inducing apoptotic cell death. The mechanism behind this effect involves the activation of apoptotic pathways, leading to the suppression of cancer cell growth. Overall, this study suggests that chitosan-coated ZnO nanoparticles (CS-ZnO-NPs) show the promising safety profiles, highlighting their potential for use in the biomedical applications.

CONFLICT OF INTEREST

The authors declare that there is no conflict of interests regarding the publication of this article.

REFERENCES

1. A. Yihun, *Emergent Mater.*, **5**, 2031 (2022); https://doi.org/10.1007/s42247-022-00427-2
2. N. Yan and X. Chen, *Nature*, **524**, 155 (2015); https://doi.org/10.1038/524155a
3. K. Rajan, K. Saravanan, K. Mohan, R. Mythili, N.I. Vatin, S. Zhang, V. Ravikumar and S. Zhang, *Polym. Adv. Technol.*, **35**, e6370 (2024); https://doi.org/10.1002/pat.6370
4. M.S. Benhabiles, R. Salah, H. Lounici, N. Drouiche, M.F.A. Goosen and N. Mameri, *Food Hydrocoll.*, **29**, 48 (2012); https://doi.org/10.1016/j.foodhyd.2012.02.013
5. D. Meng, B. Garba, Y. Ren, M. Yao, X. Xia, M. Li and Y. Wang, *Int. J. Biol. Macromol.*, **158**, 1063 (2020); https://doi.org/10.1016/j.ijbiomac.2020.04.213
6. R.S.L. Tan, P. Hassandarvish, C.F. Chee, L.W. Chan and T.W. Wong, *Carbohydr. Polym.*, **290**, 119500 (2022); https://doi.org/10.1016/j.carbpol.2022.119500
7. M. Perez, R.J.T. Endaya, F.S. Mohammad and M.C. Sepe, *Asian J. Biol. Life Sci.*, **9**, 145 (2020); https://doi.org/10.5530/ajbls.2020.9.22
8. A. Aouadi, D. Hamada Saud, A. Rebiai, A. Achouri, S. Benabdesselam, F. Mohamed Abd El-Mordy, S.F. Ahmad, S.M. Attia, H.S. Abulkhair, P. Pohl, A. Ararem and M. Messaoudi, *Sci. Rep.*, **14**, 14753 (2024); https://doi.org/10.1038/s41598-024-65579-z
9. Y. Verma, S.K. Singh, H.S. Jatav, V.D. Rajput and T. Minkina, *Environ. Geochem. Health*, **44**, 221 (2022); https://doi.org/10.1007/s10653-021-00929-8
10. M.J. Khan, S. Saeed, M. Javed and W.Q. Khan, *Glob. NEST J.*, **26**, 1 (2024); https://doi.org/10.30955/gnj.005831
11. N. Asif, M. Amir and T. Fatma, *Bioprocess Biosyst. Eng.*, **46**, 1377 (2023); https://doi.org/10.1007/s00449-023-02886-1
12. U.M.T.M. Gunathilaka, W.A.P.P. de Silva, S.P. Dunuweera and R.M.G. Rajapakse, *RSC Adv.*, **11**, 8857 (2021); https://doi.org/10.1039/D1RA00014D
13. J. Wu, C. Du, J. Zhang, B. Yang, A.G. Cuthbertson and S. Ali, *Microorganisms*, **10**, 1 (2021); https://doi.org/10.3390/microorganisms10010001
14. S. Ngasotter, K.A.M. Xavier, M.M. Meitei, D. Waikhom, Madhulika, J. Pathak and S.K. Singh, *Carbohydr. Polym. Technol. Appl.*, **6**, 100349 (2023); https://doi.org/10.1016/j.carpta.2023.100349
15. Y. Xia, D. Wang, D. Liu, Y. Guo, S. Wang, Y. Song, B. Song, Y. He and J. Wang, *Front. Bioeng. Biotechnol.*, **10**, 894667 (2022); https://doi.org/10.3389/fbioe.2022.894667
16. R.M. Saeed, I. Dmour and M.O. Taha, *Front. Bioeng. Biotechnol.*, **8**, 4 (2020); https://doi.org/10.3389/fbioe.2020.00004
17. M. Kermani, A. Mostafapour, Z. Sabouri, S.M. Gheibihayat and M. Darroudi, *Environ. Sci. Pollut. Res. Int.*, **30**, 19313 (2022); https://doi.org/10.1007/s11356-022-23518-3
18. P. Lertsutthiwong, N.C. How, S. Chandrkrachan and W.F. Stevens, *J. Met. Mater. Miner.*, **12**, 11 (2002).
19. G. Lamarque, J.-M. Lucas, C. Viton and A. Domard, *Biomacromolecules*, **6**, 131 (2005); https://doi.org/10.1021/bm0496357
20. M. Huang, E. Khor and L.Y. Lim, *Pharm. Res.*, **21**, 344 (2004); https://doi.org/10.1023/B:PHAM.0000016249.52831.a5
21. F. Buazar, S. Sweidi, M. Badri and F. Kroushawi, *Green Process. Synth.*, **8**, 691 (2019); https://doi.org/10.1515/gps-2019-0040
22. N.H. Rezazadeh, F. Buazar and S. Matroodi, *Sci. Rep.*, **10**, 19615 (2020); https://doi.org/10.1038/s41598-020-76726-7
23. M.M. AbdElhady, *Int. J. Carbohydr. Chem.*, **2012**, 563785 (2012); https://doi.org/10.1155/2012/840591
24. D. Ramimoghadam, M.Z. Bin Hussein and Y.H. Taufiq-Yap, *Chem. Cent. J.*, **7**, 136 (2013); https://doi.org/10.1186/1752-153X-7-136
25. K. Gulati, P. Bhatnagar and A. Bhatnagar, *Pesqui. Bras. Odontopediatria Clin. Integr.*, **18**, e4008 (2018); https://doi.org/10.4034/PBOCI.2018.181.50
26. A. Gizaw, L.M. Marami, I. Teshome, E.J. Sarba, P. Admasu, D.A. Babele, G.M. Dilba, W.M. Bune, M.D. Bayu, M. Tadesse and K. Abdisa, *Adv. Pharmacol. Pharm. Sci.*, **2022**, 3299146 (2022); https://doi.org/10.1155/2022/3299146
27. E. Urnukhsaikhan, B.-E. Bold, A. Gunbileg, N. Sukhbaatar and T. Mishig-Ochir, *Sci. Rep.*, **11**, 21047 (2021); https://doi.org/10.1038/s41598-021-00520-2
28. M.A. Ansari, M. Murali, D. Prasad, M.A. Alzohairy, A. Almatroudi, M.N. Alomary, A.C. Udayashankar, S.B. Singh, S.M.M. Asiri, B.S. Ashwini, H.G. Gowtham, N. Kalegowda, K.N. Amruthesh, T.R. Lakshmeesha and S.R. Niranjana, *Biomolecules*, **10**, 336 (2020); https://doi.org/10.3390/biom10020336
29. Z.U. Zango, J.O. Dennis, A.I. Aljameel, F. Usman, M.K.M. Ali, B.A. Abdulkadir, S. Algessair, O.A. Aldaghri and K.H. Ibnaouf, *Molecules*, **27**, 4746 (2022); https://doi.org/10.3390/molecules27154746
30. K.S. Kachare, S.S. Shendage, S.B. Vhanbatte, F.D. Mai and A.V. Ghule, *RSC Advances*, **14**, 33774 (2024); https://doi.org/10.1039/D4RA05950F
31. Y. Dai, Y. Zhang and Z.L. Wang, *Solid State Commun.*, **126**, 629 (2003); https://doi.org/10.1016/S0038-1098(03)00277-1
32. S.K. Mahapatra, K.A. Bogle, S.D. Dhole and V.N. Bhoraskar, *Nanotechnology*, **18**, 135602 (2007); https://doi.org/10.1088/0957-4484/18/13/135602
33. J.W. Oh, S.C. Chun and M. Chandrasekaran, *Agronomy*, **9**, 21 (2019); https://doi.org/10.3390/agronomy9010021
34. Y.H.I. Mohammed, S. Alghamdi, B. Jabbar, D. Marghani, S. Beigh, A.S. Abouzied, N.E. Khalifa, W.M.A. Khojali, B. Huwaimel, D.H.M. Alkhalifah and W.N. Hozzein, *ACS Omega*, **8**, 32027 (2023); https://doi.org/10.1021/acsomega.3c03908
35. S. Faisal, H. Jan, S.A. Shah, S. Shah, A. Khan, M.T. Akbar, M. Rizwan, F. Jan, Wajidullah, N. Akhtar, A. Khattak and S. Syed, *ACS Omega*, **6**, 9709 (2021); https://doi.org/10.1021/acsomega.1c00310
36. K. Ogawa and T. Yui, *Biosci. Biotechnol. Biochem.*, **58**, 968 (1994); https://doi.org/10.1271/bbb.58.968
37. N.J. Tamanna, M.S. Hossain, N.M. Bahadur and S. Ahmed, *Results Chem.*, **7**, 101313 (2024); https://doi.org/10.1016/j.rechem.2024.101313
38. M.F. Islam, S. islam, M.A.S. Miah, A.K.O. Huq, A.K. Saha, Z.J. Mou, M.M.H. Mondol and M.N.I. Bhuiyan, *Heliyon*, **10**, e16483 (2024); https://doi.org/10.1016/j.heliyon.2024.e25430
39. M.J.U. Rumi and M.M. Rahman, *Res. Eng. Struct. Mater.*, **10**, 165 (2023); https://doi.org/10.17515/resm2023.729ma0404
40. M. Thirumavalavan, K.-L. Huang and J.-F. Lee, *Materials*, **6**, 4198 (2013); https://doi.org/10.3390/ma6094198
41. P.R. Gandhi, C. Jayaseelan, R.R. Mary, D. Mathivanan and S.R. Suseem, *Exp. Parasitol.*, **181**, 47 (2017); https://doi.org/10.1016/j.exppara.2017.07.007
42. K. Elumalai, S. Velmurugan, S. Ravi, V. Kathiravan and S. Ashokkumar, *Mater. Sci. Semicond. Process.*, **34**, 365 (2015); https://doi.org/10.1016/j.mssp.2015.01.048

43. A.M. Pillai, V.S. Sivasankarapillai, A. Rahdar, J. Joseph, F. Sadeghfar, R. Anuf A, K. Rajesh and G.Z. Kyzas, *J. Mol. Struct.*, **1211**, 128107 (2020); https://doi.org/10.1016/j.molstruc.2020.128107
44. S. Fakhari, M. Jamzad and H. Kabiri Fard, *Green Chem. Lett. Rev.*, **12**, 19 (2019); https://doi.org/10.1080/17518253.2018.1547925
45. L. Keawchaoon and R. Yoksan, *Colloids Surf. B Biointerfaces*, **84**, 163 (2011); https://doi.org/10.1016/j.colsurfb.2010.12.031
46. S.A. Ali, E.S. Ali, G. Hamdy, M.S.E. Badawy, A.R. Ismail, I.A. El-Sabbagh, M.M. El-Fass and M.A. Elsawy, *Sci. Rep.*, **14**, 9348 (2024); https://doi.org/10.1038/s41598-024-58862-6
47. M. Jayanetti, C. Thambiliyagodage, H. Liyanaarachchi, G. Ekanayake, A. Mendis and L. Usgodaarachchi, *Sci. Rep.*, **14**, 1293 (2024); https://doi.org/10.1038/s41598-024-52014-6
48. R.S. Al-Shemary, A.M. Aljeboree and A.F. Alkaim, *Eurasian Chem. Commun. (Camb.)*, **5**, 832 (2023); https://doi.org/10.22034/ecc.2023.397277.1645
49. D. Bharathi, R. Ranjithkumar, B. Chandarshekar and V. Bhuvaneshwari, *Int. J. Biol. Macromol.*, **129**, 989 (2019); https://doi.org/10.1016/j.ijbiomac.2019.02.061
50. A. Godoy, I. Balic, A.A. Moreno, O. Diaz, C. Arenas Colarte, T. Bruna Larenas, A. Gamboa and N. Caro Fuentes, *Pharmaceutics*, **17**, 186 (2025); https://doi.org/10.3390/pharmaceutics17020186
51. H. Hsueh, W.J. Ke, C.T. Hsieh, K.S. Lin, D.Y. Tzou and C.L. Chiang, *PLoS One*, **10**, e0128457 (2015); https://doi.org/10.1371/journal.pone.0128457
52. V.B. Raghavendra, S. Shankar, M. Govindappa, A. Pugazhendhi, M. Sharma and S.C. Nayaka, *J. Inorg. Organomet. Polym. Mater.*, **32**, 614 (2022); https://doi.org/10.1007/s10904-021-02142-7
53. C.A. Fernandes, N. Jesudoss M, A. Nizam, S.B.N. Krishna and V.V. Lakshmaiah, *ACS Omega*, **8**, 39315 (2023); https://doi.org/10.1021/acsomega.3c04857
54. S.H.S. Dananjaya, R.S. Kumar, M. Yang, C. Nikapitiya, J. Lee and M. De Zoysa, *Int. J. Biol. Macromol.*, **108**, 1281 (2018); https://doi.org/10.1016/j.ijbiomac.2017.11.046
55. M.A. Asghar, F. Ahmed, A.R. Qamar, K. Khan and A. Anwar, *J. Cluster Sci.*, **36**, 47 (2025); https://doi.org/10.1007/s10876-024-02760-4
56. F. Esnaashari, H. Zamani, H. Zahmatkesh, M. Soleimani, G.A. Dashtaki and B. Rasti, *Sci. Rep.*, **15**, 3185 (2025); https://doi.org/10.1038/s41598-025-87445-2
57. S. Jayakodi, R. Shanmugam, E. Pandian, M. Govindasamy, J.M. Asiri, K.K. Yadav and J. Ryeol Choi, *Nanotechnol. Rev.*, **13**, 20240123 (2024); https://doi.org/10.1515/ntrev-2024-0123
58. M. Rajkumar, S.D. Presley, P. Govindaraj, D. Kirubakaran, F. Farahim, T. Ali, M. Shkir and S. Latha, *Sci. Rep.*, **15**, 3931 (2025); https://doi.org/10.1038/s41598-025-87932-6
59. V. Karthika, M.S. AlSalhi, S. Devanesan, K. Gopinath, A. Arumugam and M. Govindarajan, *Sci. Rep.*, **10**, 18912 (2020); https://doi.org/10.1038/s41598-020-76015-3
60. D. Solairaj, P. Rameshthangam and G. Arunachalam, *Int. J. Biol. Macromol.*, **105**, 608 (2017); https://doi.org/10.1016/j.ijbiomac.2017.07.078
61. M. Elsayed, Q.A. Alomari, A.A. Drmosh, S.A. Manda, I. Haladu and I. Olanrewaju Alade, *Opt. Laser Technol.*, **149**, 107828 (2022); https://doi.org/10.1016/j.optlastec.2021.107828
62. K. Kavithaa, M. Paulpandi, T. Ponraj, K. Murugan and S. Sumathi, *Karbala Int. J. Mod. Sci.*, **2**, 46 (2016); https://doi.org/10.1016/j.kijoms.2016.01.002
63. R. Rajendran and A. Mani, *J. Saudi Chem. Soc.*, **24**, 1010 (2020); https://doi.org/10.1016/j.jscs.2020.10.008
64. T.A. Singh, J. Das and P.C. Sil, *Adv. Colloid Interface Sci.*, **286**, 102317 (2020); https://doi.org/10.1016/j.cis.2020.102317
65. G. Venkatraman, P.S. Mohan, M.M. Mashghan, K.C. Wong, P.S. Abdul-Rahman, K.M. Vellasamy, A.H. Hirad, A.A. Alarfaj and S. Wang, *Bioprocess Biosyst. Eng.*, **47**, 1163 (2024); https://doi.org/10.1007/s00449-024-02984-8